Soja, B., Nilsson, T., Balidakis, K., Glaser, S., Heinkelmann, R., Schuh, H. (2016): Determination of a terrestrial reference frame via Kalman filtering of very long baseline interferometry data. - *Journal of Geodesy*, *90*, 12, pp. 1311—1327.

DOI: http://doi.org/10.1007/s00190-016-0924-7

Journal of Geodesy manuscript – author's version
The final publication is available at Springer via http://dx.doi.org/10.1007/s00190-016-0924-7

Determination of a Terrestrial Reference Frame via Kalman Filtering of Very Long Baseline Interferometry Data

Benedikt Soja · Tobias Nilsson · Kyriakos Balidakis · Susanne Glaser · Robert Heinkelmann · Harald Schuh

Received: 29 January 2016 / Accepted: 29 May 2016

Abstract Terrestrial reference frames (TRF), such as the ITRF2008, are primary products of geodesy. In this paper, we present TRF solutions based on Kalman filtering of very long baseline interferometry (VLBI) data, for which we estimate steady station coordinates over more than 30 years that are updated for every single VLBI session. By applying different levels of process noise, non-linear signals, such as seasonal and seismic effects, are taken into account. The corresponding stochastic model is derived site-dependent from geophysical loading deformation time series and is adapted during periods of post-seismic deformations. Our results demonstrate that the choice of stochastic process has a much smaller impact on the coordinate time series and velocities than the overall noise level. If process noise is applied, tests with and without additionally estimating seasonal signals indicate no difference between the resulting coordinate time series for periods when observational data are available. In a comparison with epoch reference frames, the Kalman filter solutions provide better short-term stability. Furthermore, we find out that the Kalman filter solutions are of similar quality when compared to a consistent least-squares solution, however, with the enhanced attribute of being easier to update as for instance in a post-earthquake period.

Keywords Terrestrial reference frame · VLBI · Kalman filter · Seismic events · Seasonal signals

B. Soja
GFZ German Research Centre for Geosciences, Potsdam, Germany
Tel.: +49 331 288-1112
Fax: +49 331 288-1111
E-mail: benedikt.soja@gfz-potsdam.de

K. Balidakis, S. Glaser, H. Schuh
Technische Universität Berlin, Institute for Geodesy and Geoinformation Science, Berlin, Germany

T. Nilsson, R. Heinkelmann, H. Schuh
GFZ German Research Centre for Geosciences, Potsdam, Germany

1 Introduction

The creation and maintenance of terrestrial reference frames (TRFs) is one of the fundamental tasks of geodesy. In the past, TRFs have usually been defined by the positions at a certain epoch and velocities of selected markers on the crust of the Earth, i.e. observing stations of the different space geodetic techniques. Primary examples are the International Terrestrial Reference System (ITRS) realizations ITRF2008 (Altamimi et al, 2011) and DTRF2008 (Seitz et al, 2012).

In addition to a linear trend, caused mostly by secular geophysical effects like plate motion and glacial isostatic adjustment, the observed station motions clearly exhibit non-linear signals, for instance due to seasonal or post-seismic effects (Krásná et al, 2015). Basically, four options exist for dealing with such signals. First of all, models to reduce these effects can be applied, such as it is done for solid Earth tides. However, the models for effects like non-tidal atmospheric pressure loading, non-tidal ocean loading, or continental water storage loading are not yet unambiguously approved and recommended by the IERS Conventions (2010). Likewise, no models are conventionally applied for any kind of post-seismic deformation. The second option is therefore to simply ignore such unmodeled effects. In this case, the unmodeled effects will show up in the residuals, but could possibly also contaminate the estimated parameters (van Dam et al, 2001). Option number three is the parameterization and the subsequent

estimatation of these signals. Since the non-linear effects reach amplitudes of several centimeters and some of them can be expressed by simple harmonics, estimating them might seem superior to ignoring them. Therefore, the different IERS (International Earth Rotation and Reference Systems Service) combination centers working on ITRF (International Terrestrial Reference Frame) solutions that include data up to the end of 2014 (such as the ITRF2014[1], released in January 2016) decided to extend the parameter space at least to include annual and semi-annual signals. However, loading deformations are often of irregular amplitude and phase and some post-seismic deformations are very complex, which challenges their parameterization. The fourth approach is based on a time series representation of estimated station coordinates. With time intervals of a few days or weeks, non-linear signals can be taken into account without parameterizing them by explicit functions. Examples of this technique are epoch reference frames (Bloßfeld et al, 2014) and TRF solutions based on Kalman filtering (Wu et al, 2015). The latter also allows for extended parameterization and is thus a mixture of option three and four.

Kalman filtering (Kalman, 1960) or other similar sequential algorithms are established techniques for parameter estimation, widely used in several geodetic fields, such as Global Navigation Satellite Systems (GNSS) positioning (e.g., Webb and Zumberge, 1993; Schüler, 2001; Li et al, 2013), combination of Earth orientation parameters (EOP, Gross et al, 1998; Gross, 2000) or gravity field determination (Kurtenbach et al, 2009). A Kalman filter approach has been successfully used by the ITRS combination center at NASA Jet Propulsion Laboratory (JPL) for their JTRF2008 solution, providing station coordinates at weekly intervals together with secular velocities and seasonal signals (Wu et al, 2015). For the analysis of very long baseline interferometry (VLBI, Schuh and Behrend, 2012; Schuh and Böhm, 2013) observations, Kalman filtering was introduced by Herring et al (1990), and recently applied in studies by Nilsson et al (2015), Soja et al (2015), and Karbon et al (2015).

The ITRF has always been a combined solution based on individual contributions of the space geodetic techniques GNSS, VLBI, Satellite Laser Ranging (SLR), and Doppler Orbitography and Radiopositioning Integrated by Satellite (DORIS), which are in turn combinations of the solutions of the different analysis centers (AC) of the respective International Association of Geodesy (IAG) services (Altamimi et al, 2002). Aside from the ITRF, also single-technique (e.g., Böckmann et al, 2010; Rebischung et al, 2012) and single-AC TRF solutions (e.g., Spicakova et al, 2011; Heinkelmann and Tesmer, 2013) are often used in the geodetic analysis as they are easier to update, a necessity for instance for new stations, after breaks caused by earthquakes, antenna repairs in the case of VLBI, or changes of GNSS antennas. However, such TRF solutions usually do not reach the accuracy and stability of ITRF due to the fact that individual technique errors are not compensated or attenuated by using other techniques that are unaffected by them (e.g., Blue-Sky effect for SLR (Sośnica et al, 2013), solar radiation pressure mismodeling for GNSS (Arnold et al, 2015)).

In this work, we investigate a Kalman filter approach for TRF determination solely based on VLBI data. However, most of our findings should be easily transferable to TRFs based on other space geodetic techniques. With a Kalman filter, it is possible to model the estimated parameters as stochastic processes, e.g. random walks, which is highly advantageous in the presence of station coordinate variations that cannot be described by linear, harmonic, or other kinds of deterministic functions. The short-term stability (meaning less scatter in the coordinate time series) can be realized by restrictive noise modeling, an advantage over epoch reference frames, for which the coordinates of each epoch are computed independently.

After introducing the data used in our study (section 2), we present our methodology (section 3) and discuss in particular the differences with respect to the approach followed at the JPL combination center. Compared to the software KALREF developed there, which uses weekly updates, our implementation supports variable time steps, depending on the availability of VLBI data. The reason is that VLBI sessions featuring a station network suitable for TRF creation are scheduled on irregular intervals from one to a few days. In our approach, it is thus not necessary to temporally interpolate the input coordinates to a specific epoch, what could be a potential error source. The derivation of the stochastic model of our Kalman filter (section 3.2) is thus different to the approach followed at JPL. While both feature site-dependent noise modeling, our software supports optional time-varying process noise during periods of post-seismic deformation (sections 3.3 & 4.2). Besides the default setup of modeling station coordinates as a random walk and estimating secular velocities (sections 3.1 & 4.1), options for using an integrated random walk for modeling station coordinates and velocities and additionally estimating seasonal signals are discussed in section 4.3. By setting the noise in the stochastic model of the Kalman filter to zero, a purely secular TRF is obtained, which we compare to a data-consistent least-squares solution as well as to

[1] http://itrf.ign.fr/ITRF_solutions/2014/

ITRF2008 (section 4.4). With the 5th section we conclude our investigations.

2 Data and preliminary analysis

2.1 VLBI data

Our Kalman filter TRF solutions are based on the observational VLBI data provided by the International VLBI Service for Geodesy and Astrometry (IVS, Schuh and Behrend, 2012), covering a period from 1980 to the end of 2013. We only use VLBI sessions with a network geometry suitable for global TRF creation and thus exclude sessions in which less than four radio telescopes participated or the volume of the polyhedron defined by the network stations is smaller than 10^{15} m^3. The resulting data set consists of 4239 VLBI sessions. Furthermore, only stations with regular observations for more than a year are considered. Therefore, only 104 out of 143 potential radio telescopes are used in our TRF solutions. The locations of these stations and their observation history are illustrated in Fig. 1. Typical for VLBI, the network is much less dense on the southern hemisphere. Only very few sites, e.g. Wettzell or Westford, have an observing period covering most of the last 35 years.

In the analysis of the individual VLBI sessions, station coordinates, radio source coordinates, EOP, tropospheric delays and gradients, as well as clock parameters are estimated with the least-squares module of VieVS@GFZ (Nilsson et al, 2015), a fork from the Vienna VLBI Software (Böhm et al, 2012). The terrestrial datum is realized by no-net translation (NNT) and no-net rotation (NNR) conditions with respect to ITRF2008 coordinates. Ten of the 104 stations are not included in the ITRF2008 and are therefore not part of the single-session datum definitions. Additionally, stations affected by earthquakes not considered in ITRF2008 are excluded from the datum after the respective events (for instance station Tsukuba after the earthquake in 2011). For the celestial datum, NNR conditions for ICRF2 (Fey et al, 2015) defining sources are applied. The analysis is performed adhering to the IERS Conventions (2010). Thus, non-tidal loading deformations due to atmospheric pressure loading, ocean loading, and continental water storage loading are not corrected for.

2.2 Geophysical loading data

We employ time series of geophysical loading deformation models to derive stochastic characteristics of station coordinates (section 3.2). These model time series are at no point used to correct the input or output station coordinate time series. We obtained all loading data in the form of displacement time series from the internet platform called International Mass Loading Service (IMLS[2]), for the same time span as the observational data, i.e. 1980 until end of 2013. The predicted displacement time series are calculated employing the spherical harmonic transform approach (e.g., Petrov, 2015) and are computed in a Center of Mass isomorphic frame.

For non-tidal atmospheric pressure loading, the displacements are obtained using the pressure anomalies given at 6-hourly intervals from MERRA (NASA, Rienecker et al, 2011). Non-tidal ocean loading displacements are derived from the ocean bottom pressure of the OMCT model (GFZ), which is forced by operational analysis of ECMWF (Dobslaw and Thomas, 2007), and is provided every six hours as well. Finally, loading displacements due to hydrological loading are based on the horizontal transport of hydrological mass from MERRA, however, at intervals of three hours. In order

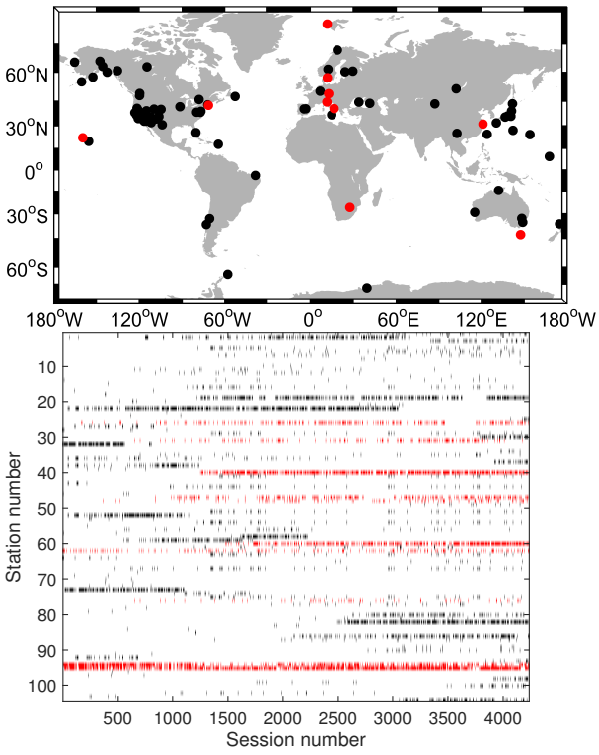

Fig. 1 Locations of the 104 VLBI stations (upper plot) and the history of their participation in the 4239 sessions (1980-2013) considered in this study (lower plot). The stations are ordered alphabetically by their 8-letter IVS names, the sessions chronologically. The ten stations used for the global datum definition are indicated by red color

[2] http://massloading.net

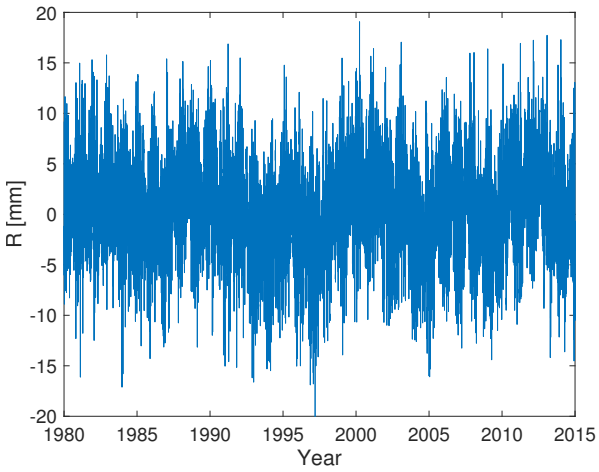

Fig. 2 Sum of the time series of non-tidal atmosphere and ocean, as well as continental water storage loading deformations at station Algonquin Park, Canada. Shown is the radial component after trend and annual signals were removed

to treat all loading constituents consistently, we only use every second value of the continental water storage loading time series.

Due to the parameterization in the Kalman filter (section 3.1), trends and annual signals are already taken into account and should not be part of the stochastic model of the coordinate offsets. Therefore, they need to be removed from the loading displacement time series. The non-tidal atmospheric pressure time series exhibit no trends due to the computation with respect to a reference pressure, but the other two loading models feature (possibly even artificial) trends. After calculating the sum of the three loading models for every station and component, we estimate their trends and annual signals and remove them from the time series. As an example, the resulting time series for station Algonquin Park, Canada, is depicted in Fig. 2. While most of the coordinate variations that reach the centimeter level seem to be of random nature, irregular signals on time scales of multiple years are present as well, which is also visible in the time series of other stations. A TRF solution based on strictly linear and harmonic functions is not able to take these variations into account.

3 Methods

3.1 Kalman filter setup

The session-wise VLBI station coordinates and their formal errors serve as the input to a Kalman filter and smoother. The formalism of the filter and smoother can be found in, e.g., Gelb (1974). The state vector $\mathbf{x}$ includes the station coordinates, velocities, and optionally parameters for seasonal signals, which for this study are assumed to be annual harmonic oscillations. The filter is updated for every VLBI session, resulting in both the state transition matrix $\mathbf{F}$ and the covariance matrix of the prediction error $\mathbf{Q}$ being time-dependent:

$$\mathbf{x}(t+\Delta t) = \mathbf{F}(t)\,\mathbf{x}(t) + \mathbf{w}(t) \tag{1}$$

$$\mathbf{Q}(t) \equiv \langle \mathbf{w}(t)\,\mathbf{w}(t)^T \rangle \tag{2}$$

Different options exist for the choice of the process noise $\mathbf{w}$. In the simplest case, it is set to zero, resulting in a TRF that is strictly linear (except for annual signals if estimated). By adding noise to the station coordinate offsets, but not to the velocities, the coordinate changes are represented by the sum of a random walk (RW) and the deterministic contribution of the velocities. For a fictitious state vector

$$\mathbf{x} = \begin{pmatrix} X \\ V_X \end{pmatrix} \tag{3}$$

just including coordinate offset and velocity in X direction for one particular station, the process noise matrix would be

$$\mathbf{Q}_{\mathrm{rw}}(t) = \Phi_{\mathrm{rw}}(t) \cdot \begin{pmatrix} \Delta t & 0 \\ 0 & 0 \end{pmatrix} \tag{4}$$

with the power spectral density (PSD) Φ_{rw} of the white noise driving the random walk and the time difference between the last and current epoch Δt. For this standard case, the noise model is derived taking into account station-dependent differences (section 3.2) and post-seismic deformations (section 3.3). Another option is to add noise to both coordinate offsets and velocities. In this case, the coordinate variations are modeled purely stochastically, and represent an integrated random walk (IRW):

$$\mathbf{Q}_{\mathrm{irw}}(t) = \Phi_{\mathrm{irw}}(t) \cdot \begin{pmatrix} \frac{\Delta t^3}{3} & \frac{\Delta t^2}{2} \\ \frac{\Delta t^2}{2} & \Delta t \end{pmatrix} \tag{5}$$

For the parameters of the optionally estimated annual signals, the noise is always set to zero, assuming that all additional position variations can be absorbed by the noise added to the coordinate offsets X. The annual signals are parameterized as oscillator processes (Chin et al, 2009; Wu et al, 2015) with the damping constant and noise set to zero.

For every station, the state vector $\mathbf{x}$ includes either six parameters (three components for coordinate offsets and velocities) or, in case annual signals are additionally estimated, twelve. By using only VLBI data and thus a limited number of stations, the computational demands are low and allow for experimentation with different filter setups.

Breaks in the coordinate time series are taken into account by increasing the process noise by several orders of magnitude so that the state estimates after the break are independent of any previous information. In case of antenna repairs or equipment changes, the process noise for velocities is kept unchanged, but for breaks due to earthquakes, both coordinate and velocity noise are inflated. The noise of the annual signal is never changed and always remains zero. In the Kalman filter, no segmentation according to breaks is done. The number of state parameters is thus independent of the number of breaks. No additional parameters or constraints, for instance for the velocity in case of an antenna repair, need to be introduced. While the smaller state vector of this approach is advantageous in terms of computational effort (in particular for multi-technique TRF solutions), creating segments and introducing additional variables after each break could help in assessing the covariance of an estimate of the size of a certain break.

The list of breaks is based on the one applied for ITRF2008. However, it has been extended to include recent events, e.g. earthquakes in Chile and Japan. Furthermore, we adapt the number of breaks depending on whether process noise is used in the filter. For instance, the complex post-seismic deformations at station Gilmore Creek, Alaska, are taken into account by introducing additional breaks (e.g. five as in ITRF2008) in the case of zero noise, while with the application of process noise a single break is sufficient.

The covariance matrix of the observations is obtained from the inverse of the squared formal errors of the input coordinates plus an additional, empirically chosen 1 cm^2 noise floor to compensate for too optimistic formal errors. The underestimation of the formal errors is for instance due to neglecting correlations between the VLBI group delay observations (e.g., Halsig et al (2014)). Tests with different observation noise floors have shown that their impact on the results is much smaller compared to tuning the process noise. The reasonable performance of the Kalman filter (cf. section 4.4) suggests that the current setup is sufficient for the kind of investigations we conduct.

ITRF2008 coordinates or, if unavailable, coordinates computed from a global VLBI solution using VieVS@GFZ (see section 3.4) are used as a priori coordinates to initialize the filter. The a priori values for velocities and annual signals are set to zero. The filter is usually run three times (forward-backward-forward), and the a priori states are updated by the last estimate when changing direction. By performing three runs, the impact of the starting values, necessary for initializing the filter in the first run, is negligible.

After all filter runs are completed, smoothed estimates of the parameters are computed as an average of the results from the last forward and backward runs, weighted by the full covariance matrices of the state vectors. The output is a filtered and smoothed time series of the coordinates of 104 VLBI radio telescopes at 4239 epochs.

In addition to the time series output, average values of the state parameters are computed by a least-squares fit to the smoothed time series. For stations with breaks, average coordinates and velocities are calculated for every segment. The sine and cosine amplitudes of the annual signals are computed from the entire time series, disregarding any breaks. Comparing the time series of parameters for which no process noise was added to a particular solution (usually velocities and oscillator parameters, for certain solutions also the coordinate offsets) with the fitted functions, the differences remain well below 10^{-3} mm or 10^{-3} mm/yr. This indicates that the filter does not suffer from numerical stability issues.

By using these average values, a datum is realized by a twelve parameter Helmert transformation with respect to ITRF2008, including translations and rotations but not the scale for the coordinates and velocities. VLBI is capable of precisely deriving the scale information from its observations. The transformation is computed based on a selection of datum sites that feature long observational history and stable behavior. In our solutions ten stations are used for the datum definition, which fulfill these criteria and exhibit a sufficiently global distribution (Fig. 1). Stations that experienced strong seismic displacements, for example in Japan or South America, have not been considered in order to prevent non-linearities from entering the datum. More stations could be used, however at the cost of settling with lower quality stations. The current set of datum stations yields acceptable results, as the comparison of transformation parameters in section 4.4 shows.

For the estimation of the transformation, the coordinates and velocities of the datum stations are assumed to be uncorrelated and of equal weight (Altamimi et al, 2002). With the transformation parameters, the coordinates and velocities of all 104 stations are then aligned to ITRF2008. This step ensures a long-term stable datum compared to the single-session datum realization which can be affected by a changing network.

In order to eliminate outliers, a test solution is computed as well as coordinate differences between the input data and this solution. If the ℓ^2-norm of the 3D coordinate difference is larger than 10 cm, the corresponding station-session pair is flagged as an outlier and eliminated in the following runs. This process is

repeated iteratively until no more outliers are detected. In total, about 200 outliers were excluded, i.e. less than 1% of the input data.

3.2 Stochastic model from geophysical deformations

In the standard case, the station coordinate offsets are modeled as random walk processes. For the determination of the PSD values Φ_{rw}, we use an approach based on non-tidal loading deformations due to mass transport in the fluid envelope of the Earth (see section 2.2).

In the input VLBI data, neither effects due to non-tidal atmosphere and ocean loading nor continental water storage loading are corrected for, although the magnitude of these deformations can exceed the centimeter level. In the Kalman filter, we do not directly apply these models either, but assume that the observed coordinate variations can be explained by these models in a stochastic sense. This allows the derivation of a station-based noise model that takes into account temporal coordinate variations of the individual sites.

To characterize the noise of station coordinates, we first compute the sum of the time series of the loading deformations due to continental water storage, non-tidal atmosphere and ocean loading effects after removing the trend and annual signal. From the resulting time series, we calculate the two-sample Allan standard deviation (ADEV) σ_y (Allan, 1966) for time lags τ between the minimum of 6 hours and 8.75 years, which is about a quarter of the total time span of the loading data we used. For example, Fig. 3 shows the ADEV for the loading time series of station Algonquin Park. The plots of other stations look very similar, with differences not in the dependency of ADEV on τ but mostly in the overall magnitude of the ADEV.

Assuming power-law noise ($\sigma_y \propto \tau^k$), it is possible to classify the type of stochastic process of the underlying time series by determining the spectral index k, which is equivalent to the slope in a log-log plot like Fig. 3. In the case of Algonquin Park, estimating k from all ADEV samples (red line) yields a value of -0.96, and also for most other stations the value is between -0.95 and -1. The latter would indicate a perfect white noise process.

Thus, one possibility would be to use white noise processes for the station coordinates in the Kalman filter. This woud be supported by Abbondanza et al (2015), who found that the noise in VLBI station coordinate time series is mostly white. However, for the application of TRF determination, a representation of station coordinates as white noise processes would be inapt since no continuity and short-term stability could

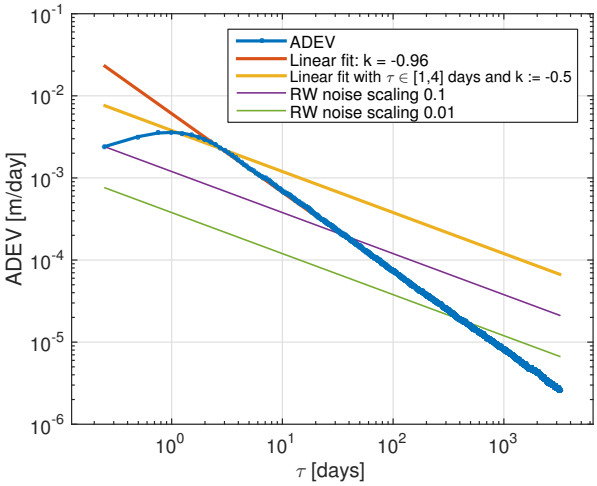

Fig. 3 Allan standard deviations (ADEV) computed from the sum of loading time series at station Algonquin Park (radial component, cf. Fig. 2) plotted against time shift τ. A fit to all ADEV samples is shown in red, one with τ between one and four days and slope k fixed to -0.5 in yellow. The thin lines correspond to the PSD derived from the yellow line being scaled by factors of 0.1 (purple) and 0.01 (green)

be realized. The parameters of every epoch would be independent of the other epochs and the solution would be similar to an epoch reference frame. A theoretical option would be to use flicker noise (f^{-1} frequency dependency), for example often found in GNSS station coordinate time series (Abbondanza et al, 2015); however, this would be very difficult and impractical to implement in a Kalman filter. For these reasons, a random walk process (f^{-2} dependency) is a much better choice and has already been successfully applied for TRF solutions (Wu et al, 2015).

It has to be noted that a random walk has more power at low frequencies compared to white or flicker noise, and therefore gives more weight to the begins and ends of the data span. With an integrated random walk (f^{-4} dependency), this effect is even larger. Still, when comparing the average velocities (basically very low frequencies) of the random walk and integrated random walk solutions (section 4.3), no significant impact can be seen.

For τ between 1-4 days, the ADEV is very close to that of a random walk process, i.e. $k = -0.5$. Since we assumed a random walk process for the coordinate model, and by taking into consideration that most time differences Δt between VLBI sessions fall exactly into this interval, it seems reasonable to use only this part from the range of ADEV samples for the computation of the PSD of the driving white noise $\Phi_{\mathrm{rw}} = \sigma_y^2(\tau) \cdot \tau$. The corresponding fit is portrayed in Fig. 3 by the yellow line.

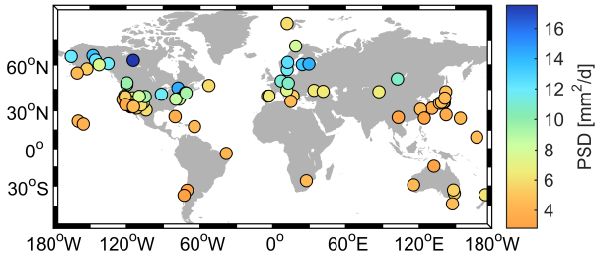

Fig. 4 Individual power spectral density (PSD) values Φ_{rw} for the radial component of 104 VLBI stations. The PSD is determined from the sum of the deformation time series due to non-tidal atmosphere and ocean, as well as continental water storage loading

Table 1 Average PSD values Φ_{rw} in mm^2/day for loading deformations of non-tidal atmosphere (NTAL) and non-tidal ocean (NTOL), as well as continental water storage (CWS) loading, split into radial, east, and north components. Additionally, the PSD values of the sum of these three loading models are included

Φ_{rw} [mm^2/day]	Radial	East	North
Sum	6.58	1.85	1.33
NTAL	4.24	0.25	0.38
NTOL	1.77	1.32	0.87
CWS	0.008	$3 \cdot 10^{-4}$	$3 \cdot 10^{-4}$

The PSD values Φ_{rw}, derived by this technique, are depicted in Fig. 4 for all 104 stations. PSD values averaged over all stations and split up into the three coordinate components are tabulated in Table 1, including those for the individual loading models. The largest process noise is, as expected, in the radial component, and primarily affected by non-tidal atmospheric pressure loading. Sites close to the sea and at lower latitudes are affected less due to the inverse barometer effect and attenuated pressure fluctuations near the equator, respectively (Wijaya et al, 2013). The PSD values of the east-west and north-south components, which are of much smaller magnitude, are mostly affected by non-tidal ocean loading. Continental water storage loading is on average close to negligible on time scales of just a few days and therefore affects the derived process noise only marginally.

With the process noise model based on geophysical loading, the filtered and smoothed coordinates are generally less noisy than the input coordinates, which are also subject to data errors or correlations with parameters like tropospheric zenith wet delays or clock offsets that are traditionally estimated in the single session VLBI analysis. Still, the variations in the filtered and smoothed coordinate time series are larger compared to the conventional TRF solutions. The overall noise level is thus a subjective choice, ranging from no noise at all (classical linear model), over the noise level derived from geophysical loading, up to closely following the session-wise coordinates (what would be similar to epoch reference frames). As both accuracy and stability are of concern in TRF solutions, a conservative compromise regarding the process noise seems reasonable. If the derivation of the noise model would be based on time intervals longer than four days while still assuming a random walk process (for example in Wu et al, 2015), the noise level would be considerably lower, as visible in Fig. 3. We have therefore opted to investigate solutions with the station-based PSD values derived from loading models scaled by factors of 1, 0.1, and 0.01.

3.3 Earthquake handling

After strong earthquakes, non-linear surface deformations with coordinate variations of several tens of centimeters can occur at observing sites close to the epicenter, e.g. at TIGO Concepción in 2010. For accurate TRF solutions it is thus imperative to model these deformation either deterministically (e.g., via logarithmic and/or exponential functions) or stochastically by adapting the process noise accordingly. We follow the latter approach and apply an additional scaling factor α to our station-based noise model depending on the time difference Δt_{eq} with respect to the epoch of the earthquake. To simplify our approach, we assume that scaling is only necessary within a period T after a major earthquake for a particular station:

$$\alpha(\Delta t_{\mathrm{eq}}) = \begin{cases} f(\Delta t_{\mathrm{eq}}) & 0 < \Delta t_{\mathrm{eq}} < T \\ 1 & \text{else} \end{cases} \tag{6}$$

We have implemented three different functions f for scaling the noise to account for post-seismic deformations, all depending on 1) an initial scaling factor α_0 that is valid right after the earthquake ($\alpha = \alpha_0$ for $\Delta t_{\mathrm{eq}} = 0$) and 2) the period T ($\alpha = 1$ for $\Delta t_{\mathrm{eq}} = T$). The function f is either exponential (Eq. 7), quadratic, or linear, as shown in Fig. 5.

$$f(\Delta t_{\mathrm{eq}}) = \alpha_0^{1-\Delta t_{\mathrm{eq}}/T} \tag{7}$$

The maximum scaling factor α_0 is chosen to be dependent on the size of the coordinate jump due to the earthquake. Before the Kalman filter and smoother is run, the coordinates of ten VLBI sessions directly before and after an earthquake are used to compute the median positions valid before and after that earthquake. For every coordinate component, the difference is calculated. As a default value, we set $\alpha_0 = 10$ for a coordinate jump of 3 m and $\alpha_0 = 1$ for 0 m, scaling

Table 2 Scaling factors α_0 for the process noise, valid right after an earthquake, are tabulated for selected stations. The values for TIGO are obtained for the 2010 Chile earthquake, the others for the 2011 Tōhoku earthquake

Station	X	Y	Z
TIGO Concepción	10.2	2.5	2.5
Tsukuba	2.2	2.7	1.1
Kashima	3.3	3.5	1.8
Mizusawa	8.5	6.1	4.6

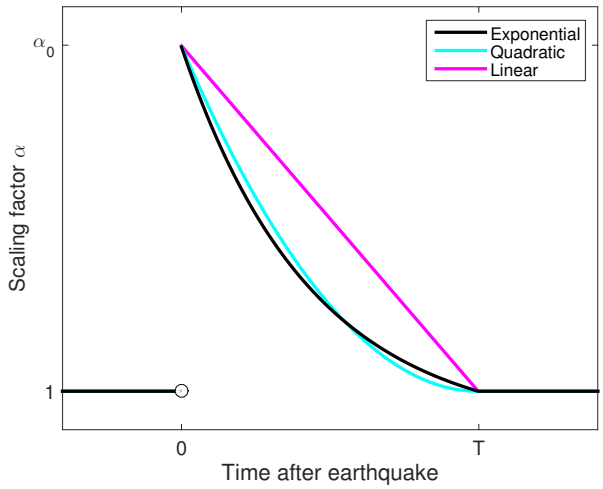

Fig. 5 Different functions for the seismic scaling factor α

linearly in between. The scaling factors are thus different for the three coordinate components. For the largest earthquakes relevant to VLBI, they can be found in Table 2. Results with different values for α_0 are discussed in section 4.2. The period T, during which the scaling is applied is set to one year for every earthquake. Of course, post-seismic deformations often last longer than that, but by a period of one year the coordinate variations are small enough that the standard process noise (cf. section 3.2) is sufficient.

The advantage of this method is that only the epoch of the main event is required as external information for post-seismic modeling, which is in any case necessary to account for the coordinate jump. The scaling factors are then calculated automatically. Geophysical information such as the magnitude of the earthquake and the distance of a station to the epicenter could be used alternatively and will be investigated by us in the future. However, the disadvantage is that all of these parameters are not necessarily correlated with the extent of the post-seismic deformation. Nevertheless, we have found our basic approach to work reasonably well (cf. section 4.2).

3.4 Least-squares TRF solution

For comparison, a TRF solution based on the same VLBI sessions and stations is determined using the software VieVS@GFZ. The main difference to the Kalman filter solutions is that free normal equation systems of all sessions are stacked and inverted in a least-squares adjustment. To solve the rank deficiency, the datum is defined by NNT/NNR conditions with respect to the same ten core stations in ITRF2008 as in the Kalman filter solutions. Likewise, the intrinsic VLBI scale is used.

3.5 Epoch reference frame solutions

In order to investigate differences between time series based TRF solutions, three epoch reference frame solutions were computed based on the same VLBI input data that were used for the Kalman filter solutions. For every interval of a certain length, the coordinates of the stations that observed during that interval were used to calculate average coordinates. The interval lengths of the three solutions were chosen as 7, 14, and 28 days. The datum is preserved from the session-wise VLBI data inversions.

4 Results and discussion

4.1 Kalman filter TRF solution

As an example, Fig. 6 depicts Kalman filter and smoother TRF solutions for station Wettzell, Germany. Here, and in all other figures of this section, the individual coordinate variations are shown in local coordinate systems. No reference solutions or trends have been subtracted, thus the plots reflect the true behavior of the coordinate variations. Besides the linear (zero noise) solution in Fig. 6, three solutions with differently scaled station-dependent noise are presented. No seasonal signals are estimated in these solutions. Despite the fact that the filtered coordinates are not as noisy as the input coordinates, still strong non-linear signals are visible at the cm level. These signals are not easily approximated by fitting harmonic functions as the amplitude strongly varies over time.

Evident is the different level of scatter for the three random walk solutions with different noise scaling factors. In particular, the solution with unscaled noise picks up a large portion of the scatter found in the input station coordinates, which is not only due to unmodeled loading displacements but also because of correlations with other parameters estimated in the VLBI analysis

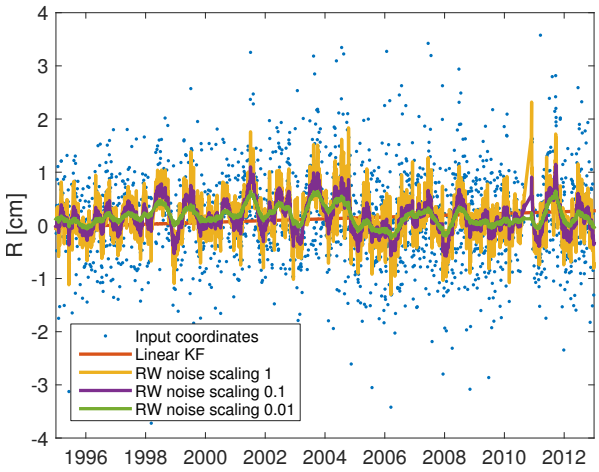

Fig. 6 Time series of radial coordinates of station Wettzell. Shown are the input coordinates (blue dots), a linear Kalman filter (KF) solution (red), and three Kalman filter solutions based on random walk processes with different levels of process noise, scaled by 1 (yellow), 0.1 (purple), and 0.01 (green)

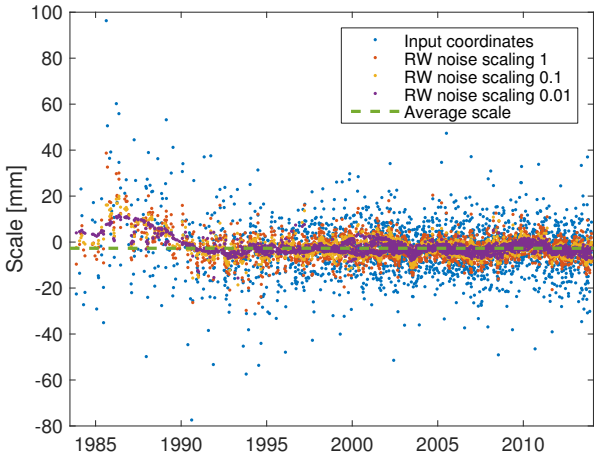

Fig. 7 Time series of scale estimates with respect to ITRF2008 based on the ten datum stations are shown for the input coordinates (blue dots) and three Kalman filter solutions based on random walk processes with different levels of process noise, scaled by 1 (red), 0.1 (yellow), and 0.01 (purple). The green dashed line represents the average scale of the three Kalman filter solutions

or effects of different observing networks. Also, the so-called analyst noise is certainly more prominent in our input data set than if it was a combination of solutions from different VLBI ACs (i.e., what is used for ITRF solutions). For these reasons, we believe that the solution with the noise level scaled by a factor of 0.1 seems to be most appropriate for our input data set. When looking at Fig. 3, the ADEV of this noise level (purple line) is on average closer to the calculated ADEV from the geophysical loading models (blue dots) over the range of considered time differences. In particular, it does not overestimate the low-frequency noise as much as the unscaled noise solution does. Still, the choice of noise level is subjective, as discussed in section 3.2. For instance, tuning down the noise level in order to mitigate artificial noise contributions might not be important when dealing with GNSS data, which usually feature smaller station coordinate scatter compared to VLBI.

In order to investigate the effects of the different noise levels on the parameters of a similarity transformation, we computed the transformation parameters with respect to ITRF2008 based on the ten datum stations for every session in which at least three datum stations participated. Datum stations that did not observe in a particular session were excluded from the calculations. In the following, we concentrate on the scale information, the most important contribution of VLBI to multi-technique TRFs, but the results are very similar for the other six transformation parameters.

In Fig. 7, the scale estimates for the same random walk solutions as in Fig. 6 are shown. Except for deviations in the 1980s, characterized by insufficient network geometries, the scale remains mostly flat. In terms of smaller variations (e.g., the bulge around 2010), all solutions show similar signals, which means that the Kalman filter maintains such information. However, the scatter is significantly reduced compared to the input coordinates, which can also be seen in the statistics from Table 3. For more homogeneous data sets, only the time period after 1994 was used to calculate the statistics. Comparing the input coordinates with the Kalman filter solution with the original noise model, a reduction of the scatter by more than 50% is seen, even more when looking at the solutions with reduced noise levels. A PSD scaling factor of ten results in about 35% smaller standard deviations (STD) of the scale time series.

Table 3 For the scale time series with respect to ITRF2008 of Kalman filter and epoch reference frame solutions (Fig. 7 and Fig. 8), biases, RMS (without subtracting a bias), and standard deviations (STD; bias subtracted) are provided in units of mm. Only data from 1994 until the end of 2013 were considered in the calculations

Scale [mm]	Bias	RMS	STD
Input coordinates	-3.4	10.8	10.2
RW noise scaling 1	-3.1	5.4	4.4
RW noise scaling 0.1	-3.0	4.1	2.8
RW noise scaling 0.01	-3.0	3.4	1.9
ERF 7 days	-2.9	7.6	6.8
ERF 14 days	-2.8	6.5	5.8
ERF 28 days	-2.9	5.9	5.2

We did the same calculations for the epoch reference frame solutions described in section 3.5. Fig. 8 features the scale estimates with respect to ITRF2008

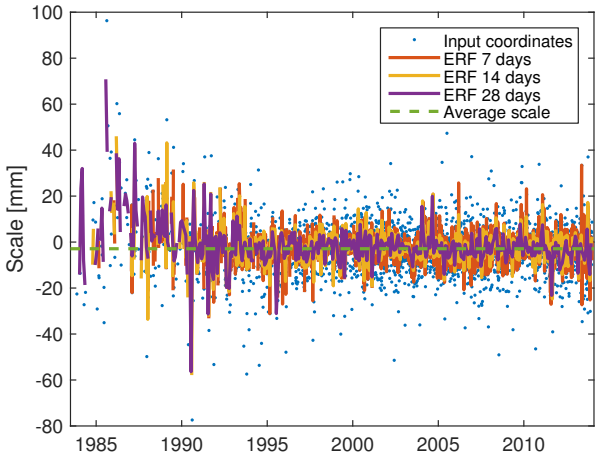

Fig. 8 Time series of scale estimates with respect to ITRF2008 based on the ten datum stations are shown for the input coordinates (blue dots) and three epoch reference frame solutions based on interval lengths of 7 days (red), 14 days (yellow), and 28 days (purple). Due to the reduced number of epochs of the latter solution, lines were used instead of points for better discernability. The green dashed line represents the average scale of the three epoch reference frame solutions

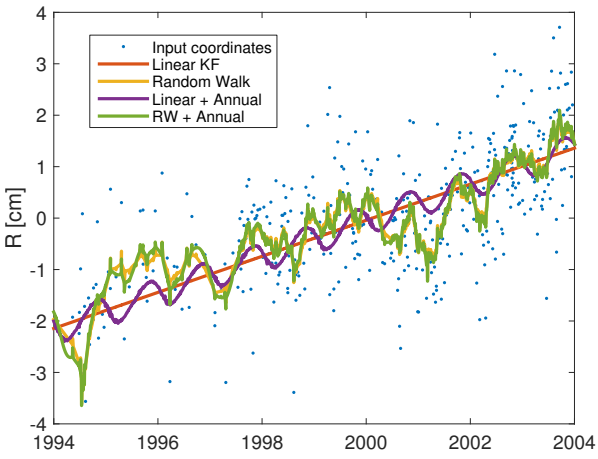

Fig. 9 Time series of radial coordinates of station Algonquin Park. Shown are the input coordinates (blue dots), a linear Kalman filter solution (red), a Kalman filter solution based on a random walk process with the process noise scaled by 0.1 (yellow), a zero noise Kalman filter solution including annual signals (purple), and a solution for which both process noise (scaled by 0.1) is applied and annual signals are estimated (green)

and Table 3 provides statistics. As expected, the scatter of the epoch reference frame solutions is smaller than for the input coordinates due to the averaging. Also, it is clearly visible that the scale variations are decreased when longer intervals are chosen. When comparing the three solutions to those from the Kalman filter, it becomes evident that epoch reference frames generally inhibit larger RMS and STD values, even when only the Kalman filter solution with unscaled noise is considered. The standard Kalman filter solution with process noise scaled by 0.1 yields STD values more than 50% smaller than those of the epoch reference solution with interval lengths of 7 and 14 days, while retaining the high temporal resolution of the input coordinates (usually 1-4 days). If the whole time span was considered instead of from 1994 onwards, the degradation of the statistics of the epoch reference frame solutions would be more severe compared to the Kalman filter solutions, since the sparse data in the early years result in the epoch reference frame coordinates often being derived just from a single session.

In Fig. 9, solutions with estimated annual signals are shown for station Algonquin Park for both linear and random walk Kalman filter setups. In the latter case, the noise is scaled by the standard value of 0.1. The amplitude of the annual signal in the radial component is about 3 mm. However, when applying process noise, it does not matter whether annual signals are estimated, as seen in the coordinate time series. The differences between the random walk solutions are marginal, which in turn differ from the pure "linear+annual" solution by sometimes more than 1 cm.

Although estimating annual signals in the presence of process noise is thus not important during times when observational data are available, it is still advantageous for predictions of future coordinates by extrapolating the deterministic model. The additional processing time required by having twice as many unknowns in the Kalman filter (or thrice in case also semi-annual signals are estimated), is bearable for VLBI only solutions. Ideally, the selection of harmonic signals to represent the coordinate time series would involve spectral analysis on a site-per-site basis. This way it would be possible to include signals with periods longer than a year as can be seen in Fig. 2.

4.2 Post-seismic deformations

Figure 10 depicts the coordinate jump and post-seismic deformation due to the 2011 Tōhoku earthquake (9.0 M_w) at station Tsukuba, Japan. At the epoch of the earthquake, for both the linear and the random walk solution, the process noise is strongly increased so that the jump can be bridged. In the case of the linear model, it becomes evident that the post-seismic deformations can not be captured well, causing differences up to 8 cm. By applying process noise, the Kalman filter more strictly follows the input coordinates. Here, the process noise after the earthquake is scaled by an exponential function (Eqs. 6 and 7, section 3.3).

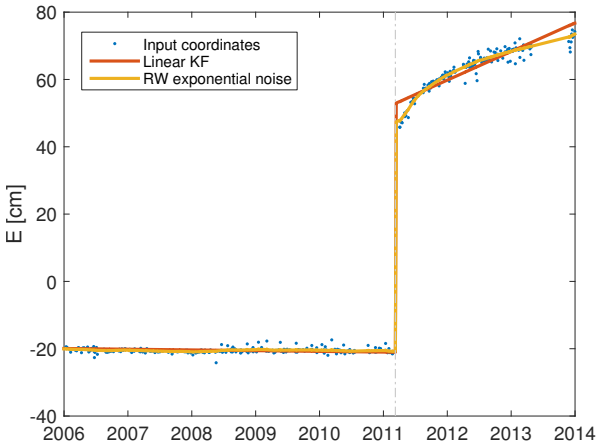

Fig. 10 Time series of east coordinates of station Tsukuba. Shown are the input coordinates (blue dots), a linear Kalman filter solution (red), and a Kalman filter solution with process noise of the random walk scaled by 0.1 and after the earthquake additionally scaled by an exponential function (yellow)

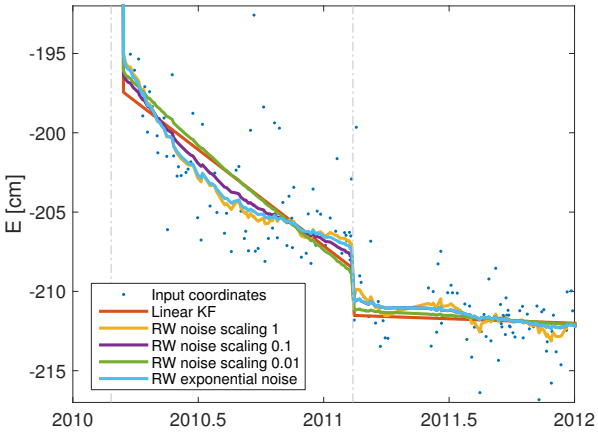

Fig. 11 Time series of east coordinates of station TIGO Concepción. Shown are the input coordinates (blue dots), a linear Kalman filter solution (red), three Kalman filter solutions based on random walk processes with different levels of process noise, scaled by 1 (yellow), 0.1 (purple), and 0.01 (green), and a Kalman filter solution with process noise scaled by 0.1 and after the earthquake additionally scaled by an exponential function (light blue)

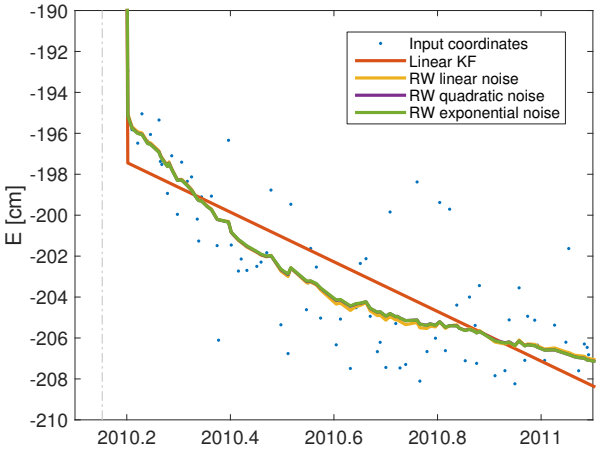

Fig. 12 Time series of east coordinates of station TIGO Concepción. Shown are the input coordinates (blue dots), a linear Kalman filter solution (red), and three random walk based Kalman filter solutions with process noise scaled by 0.1 and after the earthquake additionally scaled by different functions: linear (yellow), quadratic (purple), and exponential (green)

The other exceptionally strong earthquake affecting VLBI station coordinates took place 2010 in Chile (8.8 M_w), followed by an aftershock in 2011. In Fig. 11, Kalman filter solutions using different noise levels are shown for the station TIGO Concepción during the first years after the earthquake. For the linear solution and the one with noise scaled by a factor of 0.01, the coordinate difference to the solution with unscaled noise is up to 5 cm. A factor of 0.1 causes differences of up to 2 cm. With unscaled process noise the Kalman filter is able to capture the post-seismic deformation reasonably well, but might by too noisy otherwise (e.g. as visible in Fig. 6). By applying exponential scaling during the period after the earthquake to the random walk solution with overall noise level already scaled by a factor of 0.1, the resulting time series agrees much better with the input data in the vicinity of the earthquake and returns to a smoother pace after a few months. This can be seen well in Fig. 11, where the blue line (scaled for post-seismic deformations) first resembles the yellow one (unscaled noise) and later the purple one (noise scaled by a factor of 0.1).

Figure 12 shows the resulting coordinate time series when applying the three different scaling functions that are illustrated in Fig. 5. It becomes evident that the results are almost identical for all three scaling functions. For other stations (not shown here), the differences are even smaller. It is therefore sufficient to use the simplest one, i.e. linear scaling.

Larger is the impact of selecting different values for the initial scaling factor α_0. The default value of 10, valid for a jump of 3 m and thus for the east component of TIGO (cf. Table 2), is complemented by $\alpha_0 = 5$ and $\alpha_0 = 20$ in Fig. 13. The differences in the east coordinate of TIGO are up to 2 mm when α_0 is changed by a factor of two. Larger scaling factors let the filtered coordinates more closely follow the input coordinates. For other earthquakes and stations (not shown here), the differences are smaller.

4.3 Integrated random walk and Kalman filter velocities

Another option we have tested is the application of an integrated random walk for Kalman filter TRF deter-

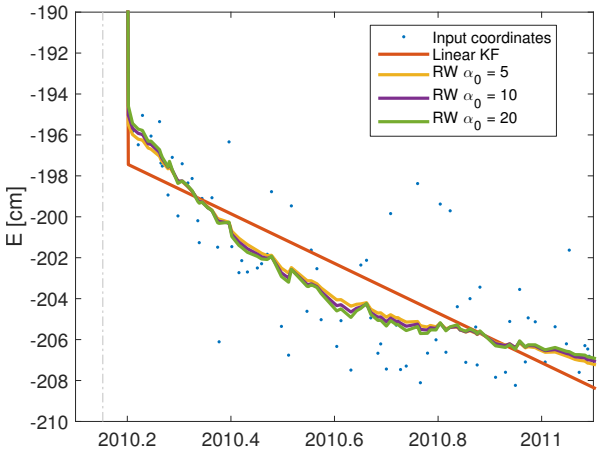

Fig. 13 Time series of east coordinates of station TIGO Concepción. Shown are the input coordinates (blue dots), a linear Kalman filter solution (red), and three random walk based Kalman filter solutions with process noise scaled by 0.1 and after the earthquake additionally scaled by functions depending on scaling factors α_0 equivalent to 5 (yellow), 10 (purple), and 20 (green)

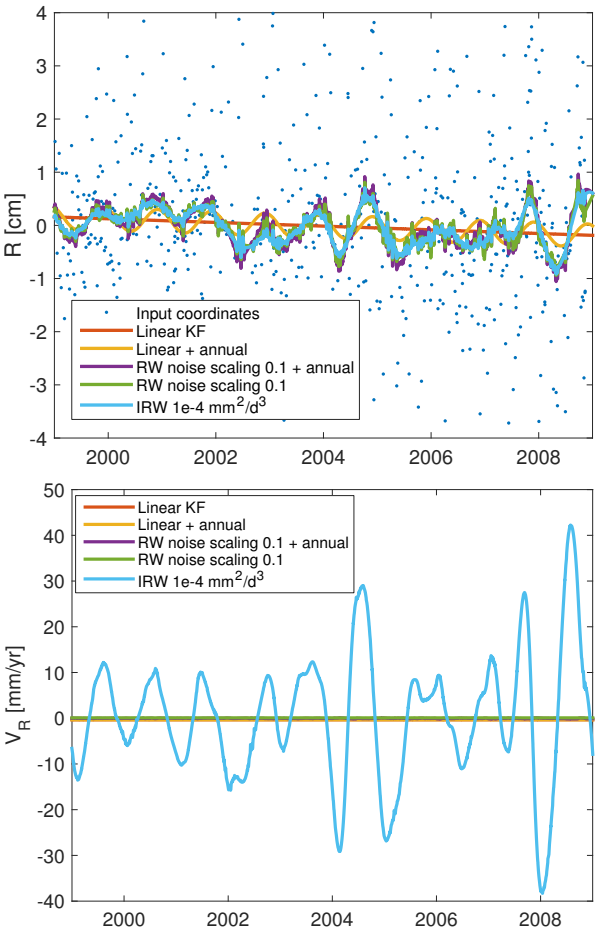

Fig. 14 Time series of radial coordinates (top) and velocities (bottom) of station Fortaleza. Shown are the input coordinates (blue dots), a linear Kalman filter solution (red), one additionally including annual signals (yellow), a Kalman filter solution based on a random walk process with the process noise scaled by 0.1 and including annual signals (purple), an identical one except for excluding annual signals (green), and a Kalman filter solution based on an integrated random walk featuring a similar noise level compared to the random walk solutions (light blue)

mination. Here, noise is added to both coordinate offset and velocity components (cf. Eq. 5). We have not derived a station based noise model for integrated random walks, but instead use an empirically chosen PSD value of 10^{-4} mm^2/day^3. In Fig. 14, we compare the integrated random walk solution with the previously investigated ones for station Fortaleza, Brazil. A very good agreement of the coordinates can be found between the solutions that use process noise larger than zero. However, the velocity time series differ appreciably because the integrated random walk approach results in instantaneous velocities, which account for short-term variations, e.g. due to seasonal signals. For certain applications, like in hydrology or volcanology, such information might be valueable. Since a constant velocity is more useful for coordinate predictions, we see not much merit in using integrated random walks for geodetic applications though. Furthermore, our investigations regarding the type of process noise (cf. section 3.2) rather support the application of a random walk. In any case, the similarity of the coordinate time series shows that the choice of process type is secondary, much more important is the selection of the overall noise level.

To investigate the impact of different choices of stochastic models and parameterizations on the average velocities, we consider the solutions presented in Fig. 14. Long-term velocities are of interest for many geophysical interpretations, e.g. regarding tectonic or post-glacial rebound effects, and are therefore sought with highest-possible accuracy. In order to reduce the amount of unsuitable stations in our velocity investigations, we only use the 74 stations that are without coordinate breaks and have observational periods longer than three years (Blewitt and Lavalle, 2002). The average velocities are computed from the Kalman filter time series as described in section 3.1. We use the linear Kalman filter solution as a reference and compute the velocity differences for all three components, from which we additionally derive 3D velocity differences: $\Delta V_{3D} = (\Delta V_x^2 + \Delta V_y^2 + \Delta V_z^2)^{-1/2}$.

Figure 15 depicts the 3D velocity differences for the 74 stations plotted against the number of VLBI sessions a station participated in. For stations with a larger number of sessions, the differences are smaller. For instance, most stations that participated in more than 500 sessions have 3D velocity differences at the 0.1 mm/yr level. Some particular stations that just par-

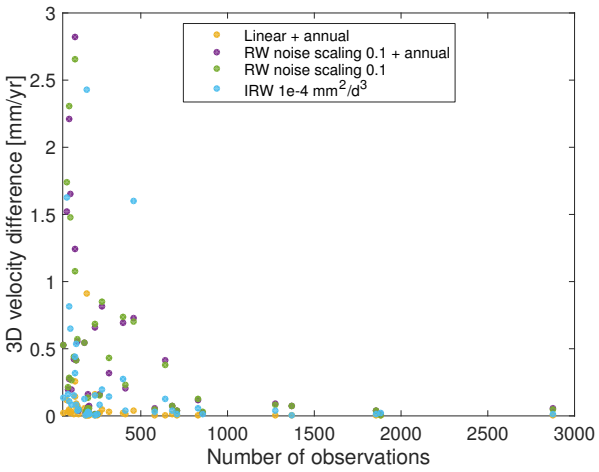

Fig. 15 Average 3D velocity differences of the solutions shown in Fig. 14 with respect to the linear Kalman filter solution, plotted against the number of VLBI sessions a particular station participated in. For better visibility, the X axis starts at 50 and the Y axis is capped at 3 mm/yr

ticipated in a few sessions have velocity differences reaching the cm/yr level (not shown in the plot). Fourteen stations participated only in ten or less stations. The reason for investigating the dependency on the number of sessions instead of the length of the observational history is that there is a much stronger anti-correlation with the velocity differences. Some VLBI stations are focused on astronomy and have only observed in a few geodetic sessions over several years. For instance, the radio telescope at Parkes Observatory, Australia, contributes to only 32 sessions distributed over 18 years in our TRF solutions. With only one or two sessions per year, the velocity is affected by different Kalman filter setups to a much larger extent compared to, for example, that of station Badary, Russia, which observed in 684 sessions during a comparatively short time of about six years.

In Table 4, we present RMS values of the velocity differences with respect to the linear KF solution. The largest differences are typically found in the radial component, which has also the largest process noise added (cf. section 3.2). The results of using all 74 stations are heavily affected by single stations with not enough observations to estimate reasonable velocities. Here, the integrated random walk solution is even closer to the linear solution than the linear-plus-annual solution. The agreement improves when only considering stations that participated in more than 200 sessions (22 stations in total). In this case, the estimation of annual signals has a very small impact on the velocities. The RMS values of all solutions that have process noise applied are almost identical. By using the standard noise level (station-based noise model scaled by 0.1), the RMS in the radial component is about 0.3 mm/yr and in the horizontal components 0.1 mm/yr.

4.4 Linear TRF comparisons

While we compared several Kalman filter solutions to a linear one in the previous section, here we want to compare the latter to other TRF solutions not based on Kalman filtering. This allows insights regarding the impact of using different estimation algorithms and datum realizations. On the one hand, we compare the linear Kalman filter solution to the data-consistent least-squares solution described in section 3.4 and, on the other hand, to ITRF2008.

In Table 5, the 14-parameter Helmert transformations between the frames are given. The parameters are estimated in an unweighted least-squares adjustment using the ten core stations with long observational history that are used for the datum definition. In the case of the least-squares solution, the transformation is based on the final TRF coordinates, but for the Kalman filter solution on the state of the solution before alignment to ITRF2008. The transformation parameters of the final coordinates of the Kalman filter solution with respect to ITRF2008 are not shown as they are below 10^{-7} mm and mm/yr (except for the scale) since the final Kalman filter coordinates and velocities are determined by applying the transformation parameters given in Table 5, excluding the scale.

The transformation parameters of the non-aligned Kalman filter solution are on average slightly larger compared to the ones obtained by the least-squares solution. Since the initial datum of the Kalman filter is only based on single-session NNT/NNR constraints, this is not surprising. Nevertheless, the differences of the transformation parameters of the two VLBI solutions with respect to ITRF2008 are within 1 σ and thus not significant. This shows that also the inherently weaker datum definition in the non-aligned Kalman filter solution yields acceptable results.

The largest differences with respect to ITRF2008 are in the scale and the Z translation. Since the scale is not included in the datum of the minimum constraint VLBI solutions and for ITRF2008 it is derived from a weighted mean of VLBI and SLR, the scale difference of about 2-3 mm is expected. It is in agreement with the ones derived by Seitz et al (2012), Table 18, and Böckmann et al (2010), Table 6. Shifts in Z direction at the millimeter level are also present in these studies. Even though the radio telescopes at the high-latitude sites Ny-Ålesund, Norway, Hartebeesthoek, South Africa, and Hobart, Australia, are part of the datum, the geometry of the VLBI network (with most stations in the

Table 4 RMS values of the velocity differences between Kalman filter solutions shown in Fig. 14 and a linear one in units of mm/yr. In the right panel, only stations that participated in more than 200 VLBI sessions are included in the computation of the RMS values

	74 stations				22 stations (> 200 obs.)			
RMS [mm/yr]	R	E	N	3D	R	E	N	3D
Linear + annual	1.65	0.64	0.52	1.85	0.03	0.01	0.01	0.04
RW noise scaling 0.1 + annual	3.52	0.88	2.61	4.47	0.30	0.12	0.09	0.34
RW noise scaling 0.1	1.26	0.56	1.48	2.02	0.31	0.13	0.10	0.35
IRW 10^{-4} mm^2/day^3	1.26	0.39	0.61	1.45	0.28	0.09	0.19	0.35

Table 5 Helmert transformation parameters (translations T, scale D, and rotations R) and their formal errors are given for a linear Kalman filter (KF) solution (before alignment to ITRF2008) and a consistent least-squares (LS) solution, both with respect to ITRF2008. The transformation parameters for the position are valid for the epoch 2005.0

KF TRF	T_X	T_Y	T_Z	D	R_X	R_Y	R_Z
Position (mm)	0.39 ± 0.83	-0.29 ± 0.85	1.86 ± 0.81	-2.18 ± 0.80	0.15 ± 1.12	-0.53 ± 0.89	0.44 ± 1.02
Velocity (mm/yr)	0.08 ± 0.09	-0.07 ± 0.09	0.01 ± 0.09	-0.05 ± 0.09	0.06 ± 0.12	-0.03 ± 0.10	0.16 ± 0.11
LS TRF							
Position (mm)	0.66 ± 0.87	0.33 ± 0.90	1.25 ± 0.85	-2.73 ± 0.84	0.00 ± 1.17	-0.01 ± 0.93	0.02 ± 1.08
Velocity (mm/yr)	-0.02 ± 0.15	-0.01 ± 0.16	-0.05 ± 0.15	0.09 ± 0.15	0.00 ± 0.20	0.01 ± 0.16	0.02 ± 0.19

northern hemisphere) may not be able to thoroughly realize the NNT condition in Z direction.

The horizontal velocities estimated in the aforementioned solutions (in the case of the Kalman filter solution after the final transformation to ITRF2008) are depicted in Fig. 16. Only segments present in all three solutions and lasting longer than three years are included. For example, for station Tsukuba, only the velocity of the segment before 2011 is shown. In general, the velocities agree well, but there are larger differences in the regions affected by seismic activity (bottom plot of this figure). A reason for some of the velocity differences could be that in our VLBI solutions, data until the end of 2013 is considered, what is not the case for ITRF2008.

In Fig. 17, the 3D velocity differences of the least-squares and Kalman filter VLBI solutions with respect to ITRF2008 are shown. Similar to section 4.3, only stations without breaks and with observational history of more than three years are considered. For the sake of comparison, stations that are not in ITRF2008 are excluded here, resulting in 64 remaining stations. Table 6 provides the corresponding RMS values. Additionally, RMS values based on 21 out of 64 stations that have observed in more than 200 VLBI sessions are included.

The differences are in general, and especially when only considering stations with good observational history, larger than those in section 4.3, indicating that the choice of estimation algorithm and datum realization weights heavier than the different ways the Kalman filter can be set up. Again, larger differences can be detected for stations with fewer observations and in the radial component. The RMS values show that the velocities of the Kalman filter solution are closer to those of ITRF2008. This could be due to the fact that both are based on input data at the solution level in contrast to the least-squares adjustment, which uses data at the normal equation level.

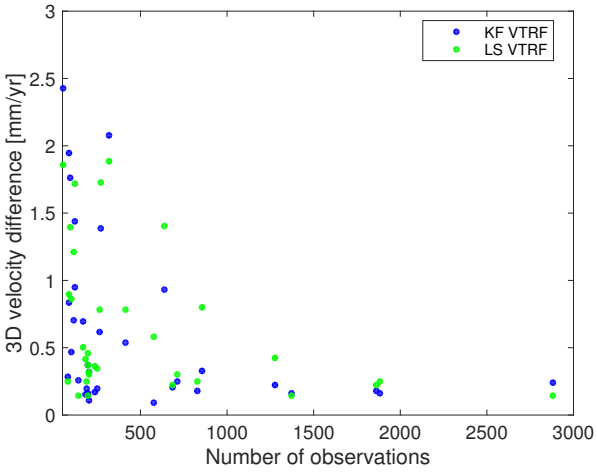

Fig. 17 3D velocity differences of linear Kalman filter (blue) and least-squares (green) VLBI TRF solutions with respect to ITRF2008, plotted against the number of VLBI sessions a particular station participated in. The axis are the same as in Fig. 15

5 Conclusions

In this paper, we have presented TRF solutions based on Kalman filtering and smoothing of VLBI data cov-

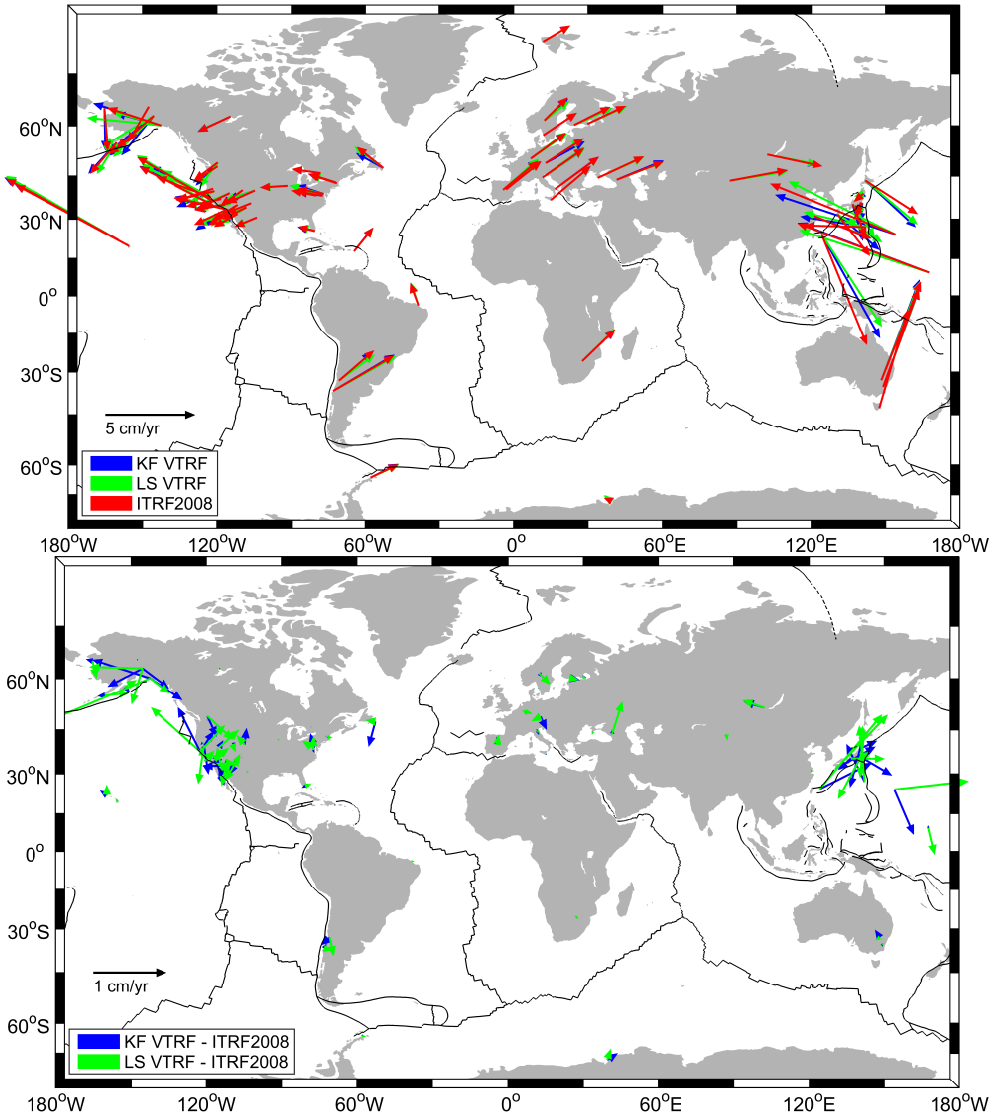

Fig. 16 Horizontal velocities (top) and their differences (bottom) obtained from consistent linear Kalman filter (blue) and least-squares (green) VLBI TRF solutions, with respect to those from ITRF2008. Only stations part of all three frames are shown

Table 6 RMS values of the velocity differences of linear Kalman filter and least-squares VLBI TRF solutions with respect to ITRF2008 in units of mm/yr. In the right panel, only stations that participated in more than 200 VLBI sessions are included in the computation of the RMS values

	64 stations				21 stations (> 200 obs.)			
RMS [mm/yr]	R	E	N	3D	R	E	N	3D
KF VTRF	3.91	1.43	1.53	4.44	1.42	0.67	0.32	1.60
LS VTRF	6.59	2.23	2.35	7.34	1.87	0.70	0.44	2.05

ering more than 30 years. The station positions are updated for every VLBI session. Estimated parameters include coordinate offsets, velocities and annual signals. By adding process noise, the coordinate variations can reflect non-linear behavior, what is especially important in case of post-seismic deformations.

In the standard case, the coordinate offsets are modeled as random walk processes with the noise model being derived station-dependent from surface loading deformation data. The largest effect contributing to the noise in the radial component is non-tidal atmospheric pressure loading, and for the lateral components non-tidal ocean loading. The process noise is inflated to

bridge breaks in the time series and to take into account strong post-seismic deformations. The type of function that is used to scale the noise during post-seismic activity is significantly less important compared to the scaling factor right after the earthquake. Our concept of adapting this earthquake-related scaling factor according to the size of the coordinate jump works reasonable well. A random walk type solution using an overall scaling factor of 0.1 for the geophysical noise model and additionally a scaling factor right after strong earthquakes of 10 for a jump of 3 m proved to be successful in our investigations.

In comparisons with epoch reference frames, the Kalman filter solutions demonstrated a better short-term stability in spite of the higher temporal resolution. In terms of scale variations with respect to ITRF2008, the standard deviation of the standard Kalman filter solution was smaller by more than 50% compared to the epoch reference frame solutions with 7 and 14 days interval length.

By testing different Kalman filter setups, we found out that if process noise is applied and observational data are available, it makes no difference to the filtered coordinate time series whether seasonal signals are estimated or not. The advantage of estimating them is therefore only a possibly improved prediction of coordinates into the future or during gaps in the observational data. Using an integrated random walk instead of a random walk, the coordinate variations show similar behavior if the process noise levels are similar. The choice of the overall process noise level has the largest impact on the Kalman filter output.

Velocities obtained from different Kalman filter setups are strongly dependent on the observational history of the stations. For stations that participated in more than 200 VLBI sessions, the RMS of the velocity differences between solutions with or without process noise is about 0.3 mm/yr. For these stations, estimating annual signals does not affect the RMS.

A linear Kalman filter solution has been compared to a data-consistent least-squares VLBI TRF solution and to ITRF2008. The differences between the transformation parameters of the two VLBI only solutions with respect to ITRF2008 have been found to be insignificant. The scales differ by 2-3 mm and the translations in Z direction differ by 1-2 mm, when compared to ITRF2008. In a velocity comparison, the Kalman filter solution was slightly closer to ITRF2008.

In the future, our Kalman filter software will be extended to estimate EOP and celestial reference frames together with TRFs. The addition and combination of other space geodetic techniques is an option as well. Regarding the datum realization, instead of estimating the transformation parameters posteriori to the filter runs, they could be added to the state vector and estimated at the same time as all other parameters. This would allow for experimentation with the process noise of the datum parameters, ranging from instantaneous to averaged transformation parameters. A different approach would be to use normal equations instead of coordinates as input data, which would then be processed by an information filter (e.g., Chin, 2001). In this case, the datum could be realized in a way similar to the least-squares solution.

Kalman filtering has been shown to be a valid tool for the delicate art of TRF creation. Station coordinates exhibit significant non-deterministic effects that can only be taken into account by stochastic modeling. Furthermore, sequential estimation algorithms like a Kalman filter allow for timely updates and might lead to TRF solutions being maintained in near real time in the future. With our study, we contribute to refining the application of Kalman filtering for TRF determination and discuss potential improvements mainly with respect to its stochastic model.

Acknowledgements The authors thank the IVS for scheduling, observing, correlating and providing the VLBI data used in this work. We thank the IMLS (http://massloading.net) for making publicly available the loading data used in this work and the IERS combination center at IGN for maintaining the ITRF. Benedikt Soja works under FWF project P 24187-N21. Furthermore, the authors want to thank the associate editor and three anonymous reviewers who helped to improve the quality of the paper.

References

Abbondanza C, Altamimi Z, Chin T, Gross R, Heflin M, Parker J, Wu X (2015) Three-Corner Hat for the assessment of the uncertainty of non-linear residuals of space-geodetic time series in the context of terrestrial reference frame analysis. Journal of Geodesy 89(4):313–329, DOI 10.1007/s00190-014-0777-x, URL http://dx.doi.org/10.1007/s00190-014-0777-x

Allan DW (1966) Statistics of atomic frequency standards. Proc IEEE pp 221–230

Altamimi Z, Sillard P, Boucher C (2002) ITRF2000: A new release of the International Terrestrial Reference Frame for earth science applications. Journal of Geophysical Research: Solid Earth 107(B10):ETG 2–1–ETG 2–19, DOI 10.1029/2001JB000561, URL http://dx.doi.org/10.1029/2001JB000561

Altamimi Z, Collilieux X, Métivier L (2011) ITRF2008: an improved solution of the international terrestrial reference frame. Journal of Geodesy 85(8):457–473,

DOI 10.1007/s00190-011-0444-4, URL http://dx.doi.org/10.1007/s00190-011-0444-4

Arnold D, Meindl M, Beutler G, Dach R, Schaer S, Lutz S, Prange L, Sośnica K, Mervart L, Jäggi A (2015) CODE's new solar radiation pressure model for GNSS orbit determination. Journal of Geodesy 89(8):775–791, DOI 10.1007/s00190-015-0814-4, URL http://dx.doi.org/10.1007/s00190-015-0814-4

Blewitt G, Lavalle D (2002) Effect of annual signals on geodetic velocity. Journal of Geophysical Research: Solid Earth 107(B7):ETG 9–1–ETG 9–11, DOI 10.1029/2001JB000570, URL http://dx.doi.org/10.1029/2001JB000570

Bloßfeld M, Seitz M, Angermann D (2014) Non-linear station motions in epoch and multi-year reference frames. Journal of Geodesy 88(1):45–63, DOI 10.1007/s00190-013-0668-6, URL http://dx.doi.org/10.1007/s00190-013-0668-6

Böckmann S, Artz T, Nothnagel A (2010) VLBI terrestrial reference frame contributions to ITRF2008. Journal of Geodesy 84(3):201–219, DOI 10.1007/s00190-009-0357-7, URL http://dx.doi.org/10.1007/s00190-009-0357-7

Böhm J, Böhm S, Nilsson T, Pany A, Plank L, Spicakova H, Teke K, Schuh H (2012) The new Vienna VLBI Software VieVS. In: Kenyon S, Pacino MC, Marti U (eds) Proceedings of IAG Scientific Assembly 2009, International Association of Geodesy Symposia, vol 136, Springer-Verlag, Berlin Heidelberg, pp 1007–1011, DOI 10.1007/978-3-642-20338-1_126

Chin T (2001) On Kalman filter solution of space-time interpolation. IEEE Transactions on Image Processing 10(4):663–666, DOI 10.1109/83.913601

Chin TM, Gross RS, Boggs DH, Ratcliff JT (2009) Dynamical and Observation Models in the Kalman Earth Orientation Filter. IPN Progress Report 42(176):24 pp.

van Dam T, Wahr J, Milly PCD, Shmakin AB, Blewitt G, Lavalle D, Larson KM (2001) Crustal displacements due to continental water loading. Geophysical Research Letters 28(4):651–654, DOI 10.1029/2000GL012120, URL http://dx.doi.org/10.1029/2000GL012120

Dobslaw H, Thomas M (2007) Simulation and observation of global ocean mass anomalies. Journal of Geophysical Research: Oceans 112(C5):11 pp., DOI 10.1029/2006JC004035, URL http://dx.doi.org/10.1029/2006JC004035, c05040

Fey AL, Gordon D, Jacobs CS, Ma C, Gaume RA, Arias EF, Bianco G, Boboltz DA, Böckmann S, Bolotin S, Charlot P, Collioud A, Engelhardt G, Gipson J, Gontier AM, Heinkelmann R, Kurdubov S, Lambert S, Lytvyn S, MacMillan DS, Malkin Z, Nothnagel A, Ojha R, Skurikhina E, Sokolova J, Souchay J, Sovers OJ, Tesmer V, Titov O, Wang G, Zharov V (2015) The Second Realization of the International Celestial Reference Frame by Very Long Baseline Interferometry. The Astronomical Journal 150(2):58, URL http://stacks.iop.org/1538-3881/150/i=2/a=58

Gelb A (1974) Applied Optimal Estimation. The MIT Press, Cambridge

Gross RS (2000) Combinations of Earth-orientation measurements: SPACE97, COMB97, and POLE97. Journal of Geodesy 73(12):627–637, DOI 10.1007/s001900050001, URL http://dx.doi.org/10.1007/s001900050001

Gross RS, Eubanks TM, Steppe JA, Freedman AP, Dickey JO, Runge TF (1998) A Kalman-filter-based approach to combining independent Earth-orientation series. Journal of Geodesy 72(4):215–235, DOI 10.1007/s001900050162, URL http://dx.doi.org/10.1007/s001900050162

Halsig S, Artz T, Leek J, Nothnagel A (2014) VLBI analyses using covariance information from turbulence models. In: Behrend D, Baver K, Armstrong K (eds) Proceedings of the Eighth IVS General Meeting, pp 272–276

Heinkelmann R, Tesmer V (2013) Systematic Inconsistencies Between VLBI CRF and TRF Solutions Caused by Different Analysis Options. In: Altamimi Z, Collilieux X (eds) Reference Frames for Applications in Geosciences, International Association of Geodesy Symposia, vol 138, Springer Berlin Heidelberg, pp 181–189, DOI 10.1007/978-3-642-32998-2_27, URL http://dx.doi.org/10.1007/978-3-642-32998-2_27

Herring TA, Davis JL, Shapiro II (1990) Geodesy by radio interferometry: The application of Kalman Filtering to the analysis of very long baseline interferometry data. Journal of Geophysical Research: Solid Earth 95(B8):12,561–12,581, DOI 10.1029/JB095iB08p12561, URL http://dx.doi.org/10.1029/JB095iB08p12561

IERS Conventions (2010) G. Petit and B. Luzum (eds.). IERS Technical Note 36, Frankfurt am Main: Verlag des Bundesamtes für Kartographie und Geodäsie

Kalman RE (1960) A New Approach to Linear Filtering and Prediction Problems. Journal of Fluids Engineering 82(1):11 pages, DOI 10.1115/1.3662552

Karbon M, Soja B, Nilsson T, Deng Z, Heinkelmann R, Schuh H (2015) Earth Orientation Parameters estimated from VLBI using a Kalman filter. Journal of Geodesy (submitted)

Krásná H, Malkin Z, Böhm J (2015) Non-linear VLBI station motions and their impact on the celestial reference frame and Earth orientation parameters. Journal of Geodesy 89(10):1019–1033, DOI 10.1007/s00190-015-0830-4, URL http://dx.doi.org/10.1007/s00190-015-0830-4

Kurtenbach E, Mayer-Gürr T, Eicker A (2009) Deriving daily snapshots of the Earth's gravity field from GRACE L1B data using Kalman filtering. Geophysical Research Letters 36(17):5 pages, DOI 10.1029/2009GL039564, URL http://dx.doi.org/10.1029/2009GL039564

Li X, Ge M, Zhang H, Wickert J (2013) A method for improving uncalibrated phase delay estimation and ambiguity-fixing in real-time precise point positioning. Journal of Geodesy 87(5):405–416, DOI 10.1007/s00190-013-0611-x, URL http://dx.doi.org/10.1007/s00190-013-0611-x

Nilsson T, Soja B, Karbon M, Heinkelmann R, Schuh H (2015) Application of Kalman filtering in VLBI data analysis. Earth, Planets and Space 67(1):136, DOI 10.1186/s40623-015-0307-y, URL http://www.earth-planets-space.com/content/67/1/136

Petrov L (2015) The International Mass Loading Service. In: International Association of Geodesy Symposia, Springer Berlin Heidelberg, in print. DOI 10.1007/1345_2015_218, URL http://link.springer.com/chapter/10.1007%2F1345_2015_218

Rebischung P, Griffiths J, Ray J, Schmid R, Collilieux X, Garayt B (2012) IGS08: the IGS realization of ITRF2008. GPS Solutions 16(4):483–494, DOI 10.1007/s10291-011-0248-2, URL http://dx.doi.org/10.1007/s10291-011-0248-2

Rienecker MM, Suarez MJ, Gelaro R, Todling R, Bacmeister J, Liu E, Bosilovich MG, Schubert SD, Takacs L, Kim GK, Bloom S, Chen J, Collins D, Conaty A, da Silva A, Gu W, Joiner J, Koster RD, Lucchesi R, Molod A, Owens T, Pawson S, Pegion P, Redder CR, Reichle R, Robertson FR, Ruddick AG, Sienkiewicz M, Woollen J (2011) MERRA: NASA's Modern-Era Retrospective Analysis for Research and Applications. Journal of Climate 24:3624–3648, DOI 10.1175/JCLI-D-11-00015.1

Schuh H, Behrend D (2012) VLBI: A fascinating technique for geodesy and astrometry. J Geodyn 61:68–80, DOI 10.1016/j.jog.2012.07.007

Schuh H, Böhm J (2013) Very Long Baseline Interferometry for Geodesy and Astrometry. In: Xu G (ed) Sciences of Geodesy II: Innovations and Future Developments, Springer-Verlag, Berlin Heidelberg

Schüler T (2001) On Ground-Based GPS Tropospheric Delay Estimation. PhD thesis, Studiengang Geodäsie und Geoinformation, Universität der Bundeswehr München

Seitz M, Angermann D, Bloßfeld M, Drewes H, Gerstl M (2012) The 2008 DGFI realization of the ITRS: DTRF2008. Journal of Geodesy 86(12):1097–1123, DOI 10.1007/s00190-012-0567-2, URL http://dx.doi.org/10.1007/s00190-012-0567-2

Soja B, Nilsson T, Karbon M, Zus F, Dick G, Deng Z, Wickert J, Heinkelmann R, Schuh H (2015) Tropospheric delay determination by Kalman filtering VLBI data. Earth, Planets and Space 67(1):144, DOI 10.1186/s40623-015-0293-0, URL http://www.earth-planets-space.com/content/67/1/144

Sośnica K, Thaller D, Dach R, Jäggi A, Beutler G (2013) Impact of loading displacements on SLR-derived parameters and on the consistency between GNSS and SLR results. Journal of Geodesy 87(8):751–769, DOI 10.1007/s00190-013-0644-1, URL http://dx.doi.org/10.1007/s00190-013-0644-1

Spicakova H, Plank L, Nilsson T, Böhm J, Schuh H (2011) Terrestrial reference frame solution with the Vienna VLBI Software VieVS and implication of tropospheric gradient estimation. In: Alef W, Bernhart S, Nothnagel A (eds) Proceedings of the 20th Meeting of the European VLBI Group for Geodesy and Astrometry, pp 118–122

Webb FH, Zumberge JF (1993) An introduction to GIPSY/OASIS-II. JPL Publ, D-11088

Wijaya D, Böhm J, Karbon M, Kràsnà H, Schuh H (2013) Atmospheric Pressure Loading. In: Böhm J, Schuh H (eds) Atmospheric Effects in Space Geodesy, Springer Atmospheric Sciences, Springer Berlin Heidelberg, pp 137–157, DOI 10.1007/978-3-642-36932-2_4, URL http://dx.doi.org/10.1007/978-3-642-36932-2_4

Wu X, Abbondanza C, Altamimi Z, Chin TM, Collilieux X, Gross RS, Heflin MB, Jiang Y, Parker JW (2015) KALREF – A Kalman filter and time series approach to the International Terrestrial Reference Frame realization. Journal of Geophysical Research: Solid Earth pp 3775–3802, DOI 10.1002/2014JB011622, URL http://dx.doi.org/10.1002/2014JB011622